CHINESE OPTICS LETTERS

Vol. 21, No. 10 | October 2023

Magnetic and electric Purcell enhancement in a hybrid metal-dielectric nanostructure

Lingxiao Shan (单凌霄)[1], Qi Liu (刘 旗)[1,2], Yun Ma (马 筠)[1], Yali Jia (贾雅利)[1], Hai Lin (林 海)[1], Guowei Lü (吕国伟)[1,2,3,4], Qihuang Gong (龚旗煌)[1,2,3,4,5], and Ying Gu (古 英)[1,2,3,4,5*]

[1] State Key Laboratory for Mesoscopic Physics, Department of Physics, Peking University, Beijing 100871, China

[2] Frontiers Science Center for Nano-optoelectronics & Collaborative Innovation Center of Quantum Matter & Beijing Academy of Quantum Information Sciences, Peking University, Beijing 100871, China

[3] Collaborative Innovation Center of Extreme Optics, Shanxi University, Taiyuan 030006, China

[4] Peking University Yangtze Delta Institute of Optoelectronics, Nantong 226010, China

[5] Hefei National Laboratory, Hefei 230088, China

*Corresponding author: ygu@pku.edu.cn

Received January 17, 2023 | Accepted May 18, 2023 | Posted Online September 6, 2023

Hybrid metal-dielectric structures combine the advantages of both metal and dielectric materials, enabling high-confined but low-loss magnetic and electric resonances through deliberate arrangements. However, their potential for enhancing magnetic emission has yet to be fully explored. Here, we study the magnetic and electric Purcell enhancement supported by a hybrid structure composed of a dielectric nanoring and a silver nanorod. This structure enables low Ohmic loss and highly-confined field under the mode hybridization of magnetic resonances on a nanoring and electric resonances on a nanorod in the optical communication band. Thus, the 60-fold magnetic Purcell enhancement and 45-fold electric Purcell enhancement can be achieved. Over 90% of the radiation can be transmitted to the far field. For the sufficiently large Purcell enhancement, the position of emitter has a tolerance of several tens of nanometers, which brings convenience to experimental fabrications. Moreover, an array formed by this hybrid nanostructure can further enhance the magnetic Purcell factors. The system provides a feasible option to selectively excite magnetic and electric emission in integrated photonic circuits. It may also facilitate brighter magnetic emission sources and light-emitting metasurfaces with a more straightforward design.

Keywords: Purcell effect; magnetic emission; hybrid structures.
DOI: 10.3788/COL202321.103602

1. Introduction

At present, the magnetic Purcell effect[1] is receiving more attention in photonic applications, particularly in optical antennas[2] and metamaterials[3], which enables further employment and characterizing of magnetic emission in nanophotonic structures[4]. In common systems, the strength of the magnetic dipole transitions is usually weaker than the electric dipole transitions by several orders[5]. But some emitters, such as lanthanide ions[6] and quantum dots[7], have considerable magnetic dipole magnitudes[8] within the optical range, allowing them to act as magnetic quantum emitters (MQEs). To maximize the magnetic Purcell effects, it is crucial to use nanostructures that support strong magnetic resonances. Metallic split-ring resonators[9,10], dielectric nanospheres[11], dielectric nanodisks[12,13], dimer antennas[2,14], diabolo antennas[15,16], and nanohole (or nanoparticle) arrays[3,17] have been investigated for providing magnetic resonances with a high magnetic density of states (MLDOS).

The nanostructures mentioned above are made of only dielectric or metal, each possessing intrinsic advantages and disadvantages. Dielectric nanostructures exhibit low intrinsic loss and high radiation directivity but offer weaker field enhancement, while metal ones have ultrastrong field confinement but suffer from substantial Ohmic loss. Nevertheless, hybrid nanostructures can achieve the balance between low loss (higher quality factors) and high confinement (smaller mode volumes). By controlling the size, shape, and composition of the hybrid structures, researchers can tailor the properties of the hybrid resonance to meet specific requirements, offering a promising avenue for the development of high-performance nanophotonic devices. Multilayer nanodisks[18], nanodisk-nanoparticle structures[19,20], dimer antennas[21], Yagi–Uda antennas[22],

nanoparticle-cavity systems[23–26], metal-semiconductor nanowires[27,28], and hybrid gratings[29] have been discussed in previous work. These nanostructures have exhibited their potentials in nanolasers[30,31], strong light–matter interaction[24,26], radiation directivity control[32,33], nonlinear effects[20,34,35], and sensing[36]. But these hybrid structures are mostly employed in producing considerable electric Purcell enhancement[37]. The magnetic Purcell enhancement, though important, has been rarely studied. Their potential in enhancing the magnetic Purcell effect needs further investigation via combining the advantages of dielectric and metal materials.

In this work, we propose a hybrid structure, including a dielectric nanoring and a metal nanorod. The structure can efficiently enhance the emission from both magnetic and electric dipole transitions within the optical communication band. Strong magnetic and electric optical resonances are both supported in our hybrid structure. Compared to a single nanoring or nanorod, the hybrid structure yields the higher magnetic (∼60) and electric Purcell factors (∼45). The structural parameters offer many freedoms that can be adjusted for much higher Purcell enhancement. Moreover, the Ohmic loss is also low in the hybrid resonances. Our structure also exhibits a high radiation efficiency of over 95%, which may benefit far-field radiation manipulations. We find that the positions of magnetic (MQE) or electric quantum emitters (EQE) can range in a large region. The finding allows for more flexibility in experimental fabrications. Furthermore, when the hybrid structures are arranged in an array, the MQE can yield a larger Purcell enhancement. The structure provides an option of having photon sources with selective excitations of magnetic and electric emission[38]. Such selective excitation can enhance and even monitor certain photochemical reactions, which only happens when magnetic dipole transitions are excited[39,40]. For example, singlet oxygen-mediated photoadditions can be improved through this method. The resonance wavelengths of magnetic and electric emission can be tuned to suit specific molecules. The hollow and gap regions also offer suitable positions to adsorb molecules. The hybrid structure can also boost novel applications, such as light-emitting metasurfaces and optical antennas for magnetic emission.

2. Model Setup

The resonances in our hybrid structure originate from the hybridization of a silicon nanoring and a silver nanorod. For the single nanoring or nanorod, the magnetic dipole (MD) resonance of the nanoring[12] and the electric quadrupole (EQ) of the nanorod[41] are both located at 1360 nm. These resonances enable very strong magnetic or electric resonances so that the emitter can yield very high Purcell enhancement around the nanoring or the nanorod. Under the mode hybridization, the hybrid resonances appear at 1305 and 1430 nm, which demonstrate high magnetic and electric density of states (MLDOS and ELDOS), respectively. Moreover, the Ohmic loss is suppressed. Thus, the greater magnetic and electric Purcell enhancements can be achieved along with a high radiation efficiency. Particularly, the magnetic Purcell factor approaches 60, and the radiation efficiency remains steady above 95%. The large MLDOS are distributed in the region around the nanoring. The emitter can thus be positioned in relaxed fabrication requirements. Moreover, a 40-fold Purcell enhancement can be achieved in the gap between the nanoring and the nanorod. By narrowing the gap, the electric emission enhancement can be higher.

The hybrid structure consists of a silicon nanoring and a silver nanorod on a silica substrate, as shown in Fig. 1(a). The two components are separated by a gap with $g = 70$ nm (10–200 nm is suitable for high Purcell enhancement). An emitter is set at 55 nm above the substrate (ranging from 0 to 150 nm in the discussion section). The entire system is exposed in the air. The outer radius and inner radius of silicon nanoring are $r_{out} = 225$ and $r_{in} = 110$ nm, respectively. Its refractive index is $n_{ring} = 3.7$. The silver nanorod has a length of $l_{rod} = 870$ nm and a width of $d_{rod} = 150$ nm. Its permittivity is adopted from the data measured by John and Christy[42]. The height of both components is $h = 110$ nm. The height of the silica substrate is set as $H_{sub} = 100$ nm with its refractive index $n = 1.48$ (ranging from 1 to 3 in the discussion).

The electromagnetic simulation is conducted in the commercial COMSOL software using finite element analysis. The size of the simulation module is 2700 nm × 2700 nm × 2100 nm. A 150-nm perfectly matched layer is set at the boundary to simulate an infinite space. The substrate is located in the middle, and two 1-μm air layers are set in the top and bottom. The air and substrate are equipped with meshes of 70 and 50 nm, respectively. The nanoring and nanorod have a finer mesh of

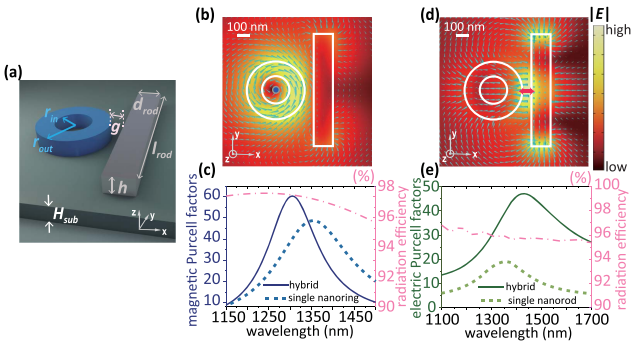

Fig. 1. (a) Schematic of our hybrid structure consisting of a silicon nanoring, a silver nanorod, and a silica substrate. Structural parameters are ticked out in the illustration. (b) Field profile of the magnetic-like resonance excited by the MQE (ticked out by a blue dot). (c) Purcell factor (solid line) and the radiation efficiency (pink dashed line) under the excitation of the MQE. The Purcell factors of a single nanoring are illustrated by a blue dashed line. (d) Field profile of the electric-like resonance excited by the EQE (ticked out by a dark red arrow). (e) The Purcell factor (solid line) and the radiation efficiency (pink dashed line) under the excitation of the EQE. The Purcell enhancement of a single nanorod is illustrated by a green dashed line. Cyan arrows depict the electric field around the hybrid structure in (b),(d).

20 nm. To calculate the total power, a 4-nm sphere surrounding the emitter is applied. Its mesh size is 2 nm. The total power is acquired by the energy flux integration on the sphere, $P_{\text{tot}} = \oiint \vec{S} \cdot d\vec{A}$. The magnetic (electric) Purcell factor is calculated by $F_{M(E)} = P_{\text{tot}}/P_{M(E)}$. $P_{M(E)}$ and represents the emitted power in the vacuum of the MQE (EQE). The power of the far-field radiation is calculated by the power flux integration on the boundaries surrounding the module.

3. Magnetic and Electric Purcell Enhancement in the Hybrid Structure

3.1. Resonances in the hybrid structure

Our hybrid metal-dielectric structure supports the hybrid magnetic-like and electric-like resonances stemming from the MD and the EQ resonances in a single silicon nanoring and silver nanorod. Here, we set the resonances of a single nanoring or nanorod at 1360 nm (structural parameters can be found in the model setup above. More details are shown in the Supplementary Material). For the silicon nanoring, the MD resonance dominates at 1360 nm. It can provide high Purcell enhancement when the MQEs locates in the center[12]. For the silver nanorod, only the electric resonances are supported. The rod length is chosen as 870 nm with the EQ resonance dominating. EQEs can yield strong Purcell enhancement in the setup[41]. Superior to the single nanoring and nanorod, our proposed structure enables hybrid resonances with a further increase of local density of states (LDOS) along with low Ohmic loss.

When the two components are put together, two hybrid resonances move apart from the original MD and EQ resonances. The first is the magnetic-like resonance at 1305 nm [Fig. 1(c)]. It is excited by the MQE at the center of the nanoring. The emitter is 55 nm above substrate, whose polarization is perpendicular to substrate. Figure 1(b) demonstrates that the nanoring exhibits a strong MD field pattern. Due to the near-field coupling in the gap, the EQ on the rod is suppressed since its field pattern is perpendicular to the gap and does not overlap with the MD on the nanoring. Thus, the rod is only excited with the field pattern of the ED. Figure 1(c) reveals a larger magnetic Purcell enhancement in the magnetic-like resonance, and the emission linewidth is also reduced compared to the single nanoring. This phenomenon can be interpreted as a result of the coupling between the nanorod and the nanoring. With a relatively weak excitation, the nanorod acts as a reflector rather than a resonator[43]. The hybrid system can be seen as a combination of two nanorings with MDs on them. The hybrid resonance based on two MD resonances can support narrower linewidth and higher magnetic Purcell enhancement[2]. For the electric-like resonance located in 1430 nm, its field profile indicates a pattern of the EQ in the nanorod, while the nanoring has a weaker excitation of the ED. Because of the high field confinement of the gap surface plasmons, the electric-like resonance can support the strong electric Purcell enhancement, which surpasses the emission enhancement with a single nanorod [Fig. 1(e)].

3.2. Magnetic and electric Purcell enhancements

We then investigate the magnetic or electric Purcell effects when the MQE or the EQE is situated at the different points of the hybrid nanostructure. For the magnetic Purcell effect, the MQE is located in the hollow region of dielectric nanoring, and its orientation is normal to the substrate. Such a setup can maximally excite the magnetic-like resonance[12,44] and surpasses the Purcell factor obtained in a single nanoring. Compared with the relevant work aimed at enhancing magnetic Purcell effects, the level of our hybrid structure is superior or comparable to dielectric nanospheres[11], metal diabolo antennas[16], and metal nanodisk arrays[45]. Additionally, the distance (55 nm) between the emitter and the structure is larger than the research above under similar Purcell enhancement, which brings convenience to nano-assembling. As shown in Fig. 1(c), the magnetic Purcell factor reaches a peak of 59 at 1305 nm [Fig. 1(c)] when the MQE is located at 55 nm above the substrate. Compared with the single nanoring, the Purcell enhancement has a higher peak along with a narrower linewidth in the hybrid structure. The higher and narrow-linewidth magnetic Purcell enhancement also originates from the mode coupling in the magnetic-like resonance, which can be seen as the coupling of two MDs on the nanoring. A similar situation was discussed in the metal-dielectric photonic structures[2,43]. At a particular gap width, the magnetic Purcell factor can be maximized, which will be discussed in Section 3.3. To characterize the radiation property of the hybrid structure, we adopt a radiation efficiency of $\eta = P_{\text{rad}}/P_{\text{tot}}$ by measuring the portion of the radiated power to the far field. As shown with the purple line in Fig. 1(c), over 90% of the emission from the emitter can be transmitted to the far field region. The Ohmic loss is suppressed because of the weak excitation of the nanorod.

For the electric Purcell effect, the EQE is located in the middle of the gap. Its dipole orientation is normal to the nanorod, corresponding to the hotspot of the EQ resonance [Fig. 1(d)]. The two structures form a gap plasmon with a large ELDOS[46], resulting in greater Purcell enhancement compared with a single nanorod. As the gap decreases, the electric Purcell factor displays a dramatic rise, which will be discussed in the following section. The peak of the electric Purcell factor is 46 at 1430 nm. Importantly, the radiation efficiency keeps at a very high level above 95% [Fig. 1(e)], which is useful for far-field light manipulations. The suppression of Ohmic loss can be attributed to the ultra-confined resonance with the existence of low-loss dielectric materials[47]. In our hybrid structure, the MQE and the EQE excite highly-confined resonances with low absorption, resulting in both a strong magnetic and electric Purcell enhancements along with a high radiation efficiency. These advantages of the hybrid structure may advance efficient nanoscale photon sources with a simpler arrangement.

3.3. Influence of structural and material parameters on Purcell factors

In the following section, we discuss the influence for Purcell enhancement under the variations of structural and material

parameters. Here, the gap width g modulates the magnetic and electric-like resonances. g should be set around 70 nm for achieving both high magnetic and electric Purcell enhancements. The substrate refractive index n influences the coupling between the nanostructure and the substrate. When n increases, the Purcell factors will experience a slight transition with a red shift of resonance. The inner radius r_{in} of the nanoring can effectively enhance the magnetic Purcell effect, and the electric Purcell effect has a slight change under the increasing r_{in}. The rod length l_{rod} also modulates the hybrid resonances by changing the field pattern of the nanorod. In our hybrid structure, these parameters provide a wealth of freedom to modulate the Purcell effect and the resonance wavelengths. These freedoms can provide more possibilities in controlling emission on integrated circuits.

When the gap width g varies, the LDOS in the two hybrid resonances are modified. The optimal choice of g is around 70 nm. Such a setup is suitable for both high magnetic and electric Purcell enhancements. For the magnetic-like resonance [Fig. 2(a)], the variation with the gap width is closely related to the coupling of the MD on the nanoring and the ED on the nanorod. When the gap is below 50 nm, the MD-ED near-field coupling is very strong. The field confinement is weakened, which produces a broader emission linewidth and pushes the magnetic-like resonance to shorter wavelengths[2]. Additionally, the magnetic Purcell factors are lower. When the gap width is moderate, the ED on the nanorod is relatively weak, and the nanorod acts more as a reflector than a resonator. The hybrid resonance becomes a coupling of two nanorings with MDs on them. The magnetic Purcell factor displays an increase in this situation. As the gap keeps increasing, the MLDOS reduces to the level of a single nanoring, and the resonance wavelength has a red shift. The maximized magnetic Purcell enhancement is 64 at $g = 100$ nm. In order to obtain the largest MLDOS, the gap width should be moderate, while for the electric-like resonance, the narrower gap brings much higher Purcell enhancement, as shown in Fig. 2(b). The ultrahigh ELDOS originates from the ultra-confined gap plasmon systems[46]. Particularly, the Purcell factor approaches 680 at a wavelength of 1500 nm when $g = 10$ nm. Such enhancement is at the same level as that in all-metal two-layer diabolo antennas[16]. The resonance wavelength has a red shift when g shrinks below 20 nm.

The refractive index n of the substrate has a significant influence on the coupling between the nanostructure and the substrate. Therefore, the Purcell factor can be modulated. When n increases, the magnetic-like resonance experiences a red shift, and the peak values of the Purcell enhancement declines [Fig. 2(c)]. The maximal magnetic Purcell enhancement drops from 68 to 40 when n ranges from 1 to 2.5. This is because the approaching refractive index between the nanoring and the substrate induces the field extension into the substrate. The extension changes the confined field pattern around the nanostructures and then pushes the resonances to longer wavelengths, while for the electric-like resonance, the Purcell enhancement has only a slight rise with the increasing n. But the range of the red shift of the resonances reaches about 400 nm when n ranges from 1 to 2 [Fig. 2(d)]. The substantial red shift can be attributed to the stronger hybridization of the nanorod and the substrate[48,49].

The inner radius r_{in} of nanoring can strongly modulate and enhance the magnetic Purcell effect. The phenomenon was investigated in the single dielectric nanoring[12], which also works in our hybrid structure [Fig. 2(e)]. When r_{in} decreases, the magnetic Purcell factor can be largely enhanced, and the resonance wavelength experiences a red shift. At $r_{in} = 20$ nm, the peak Purcell factor can be larger than 200, while for the electric Purcell effect [Fig. 2(f)], the decrease of r_{in} slightly changes the peak Purcell factor and brings a blue shift of the resonance.

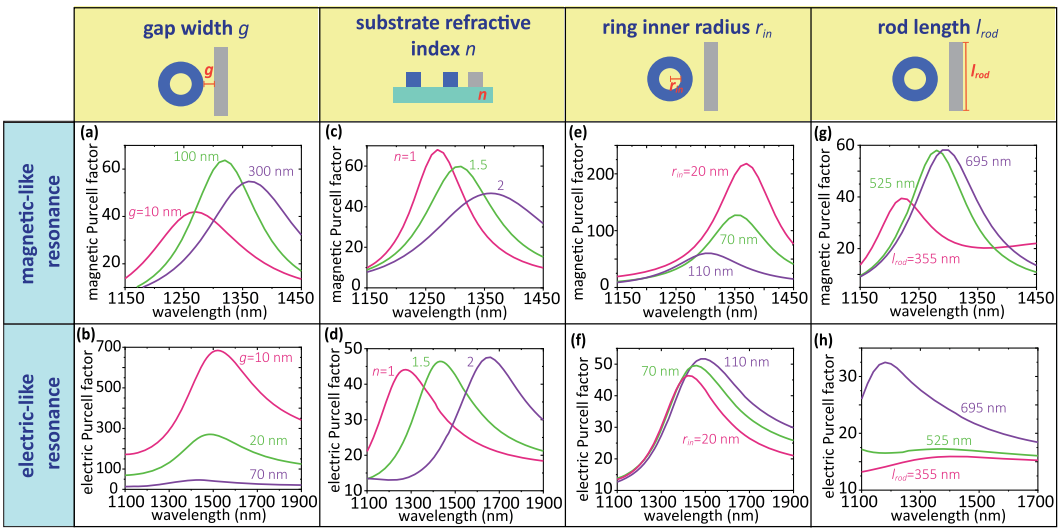

Fig. 2. Variations of the magnetic and electric Purcell enhancement under some structural parameters in the magnetic (electric)-like resonance. Magnetic and electric Purcell factors as a function of (a),(b) gap width g, (c),(d) substrate refractive index n, (e),(f) inner radius of the nanoring r_{in}, and (g),(h) length of nanorod l_{rod}.

The rod length l_{rod} alters the hybrid resonance mainly by changing the excitation situation on the rod. For the magnetic-like resonance, the rod demonstrates a pattern of ED as mentioned in Section 3.1. When the rod length is shorter, the ED is close to the resonance ($l_{rod} = 355$ nm) so that the MD-ED coupling is obvious, which produces the broader emission linewidth and the blue shift of the resonance wavelength. When the rod is longer, the rod has a weaker field and acts as a reflector. As seen in Figs. 1(c) and 2(g), the hybrid resonance is only slightly influenced by the increasing l_{rod} ranging from 525 to 870 nm. For the electric-like resonance, the rod length changes the field pattern on the nanorod. While the ring is only weakly excited. When the rod length decreases, the resonance of the electric quadrupole on the rod has a blue shift and gradually disappears at a very short rod length. This phenomenon induces the blue shift of the electric-like resonance [Fig. 2(h)] and diminishes the Purcell factor.

3.4. Insensitivity of the Purcell factors to the emitter's position

In the following, we investigate the influence of the emitter's position on the Purcell factors. Our findings reveal that the Purcell factor remains high within a range of several 100 nm in the near-field region. Interestingly, the deviation of the emitter from the center of the nanoring or the gap can bring even higher magnetic and electric Purcell enhancements. These results demonstrate the flexibility in our hybrid nanostructure and thus provide more convenience in nano-fabrications. The large magnetic Purcell enhancement can be achieved inside the nanoring and in the hollow region[50], while the electric Purcell enhancement keeps a high level when the EQE locates around the nanorod[41]. These hotspots of enhancement also correspond to the field hotspots in magnetic and electric-like resonances [Figs. 1(b) and 1(d)].

Considering the magnetic Purcell effect, the Purcell factors keep at a high level around the nanoring. Figure 3(a) displays the Purcell factors when the MQE moves through a path through the center of the nanoring and normal to the nanorod. The Purcell factor reaches maximums around 90 at inner boundaries. A similar situation also manifests in Fig. 3(b). The deviation from the center does no harm to but benefits the higher emission enhancement. Moreover, the Purcell factors remain steady at 60 when the MQE intrudes into the nanorod. Figure 3(c) reveals the transition of the Purcell factor when the distance to the substrate of the MQE changes. The MQE can be placed at 50 nm above the substrate where the Purcell factor reaches the maximum of 60. When the MQE is closer to the substrate or comes into the substrate, the Purcell factor exhibits a decrease.

The electric Purcell enhancement is also insensitive to the position of the EQE and remains high when the EQE lies around the nanorod. In Fig. 3(d), there is nearly no ELDOS enhancement when the EQE is close to the nanoring. On the contrary, the Purcell factor of the EQE increases in the vicinity of the nanorod[51]. We find that the electric Purcell factor approaches 70 at the nanorod boundaries. In Fig. 3(e), the EQE yields the highest Purcell factor of 45 at the gap center. For both the large Purcell enhancement and experimental practicability, the EQE is suitable to locate in the gap. Note that in real experiments, it cannot be positioned too close to the nanorod boundary because it may induce quantum effects[52,53], which is not included in the electromagnetic simulation. Figure 3(f) reveals the influence of the distance from the substrate. The trend of the Purcell enhancement is similar to that of the MQE. The largest enhancement appears at 40 nm above the substrate, and when the EQE moves down into substrate or away from structure, the Purcell factor will drop.

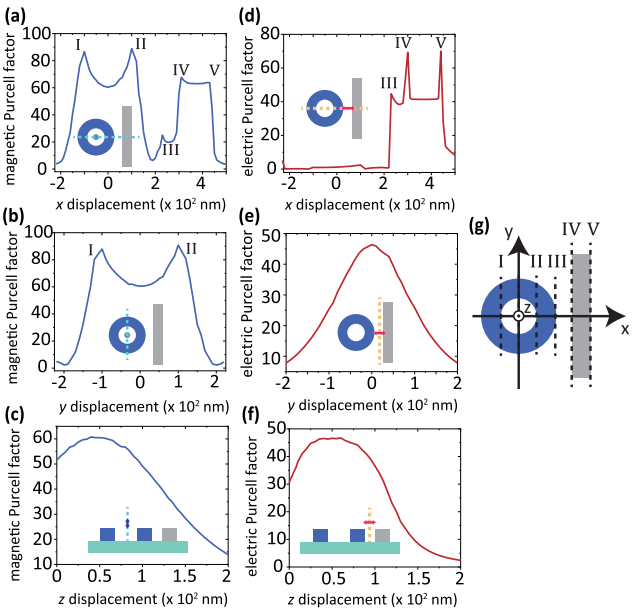

Fig. 3. Variation of the magnetic and electric Purcell enhancement when the emitter's position moves. (a)–(c) Magnetic Purcell factors when the MQE moves along the three paths depicted in the insets. The MQE feels the strongest emission enhancement at the inner boundaries. (d)–(f) The electric Purcell factors when the EQE moves along 3 paths depicted in the insets. The peak enhancement appears at the boundary of the nanorod. (g) Illustration of some specific points. The origin is set at the center of the nanoring and on the substrate. Some specific positions are also ticked out by Roman numerals I–V.

4. Magnetic and Electric Purcell Enhancement and Far-Field Radiation in an Array

In this section, we explore the emission properties in an array composed of the hybrid structures [Fig. 4(a)]. The emission of a single MQE or EQE can be modulated under the hybrid resonance joined by the array cells. For the emission enhancement, the magnetic Purcell factor is even larger than that in the individual structure. The far-field radiation from the MQE also exhibits a high directivity. Every cell in the array is an individual hybrid metal-dielectric structure with the same setup as above. The intervals between rows and columns are $d = 1000$ nm. A 9×9 array is simulated, and its size is $9650\ \text{nm} \times 9650\ \text{nm} \times 2100$ nm. Only one MQE or EQE is set to excite the entire array.

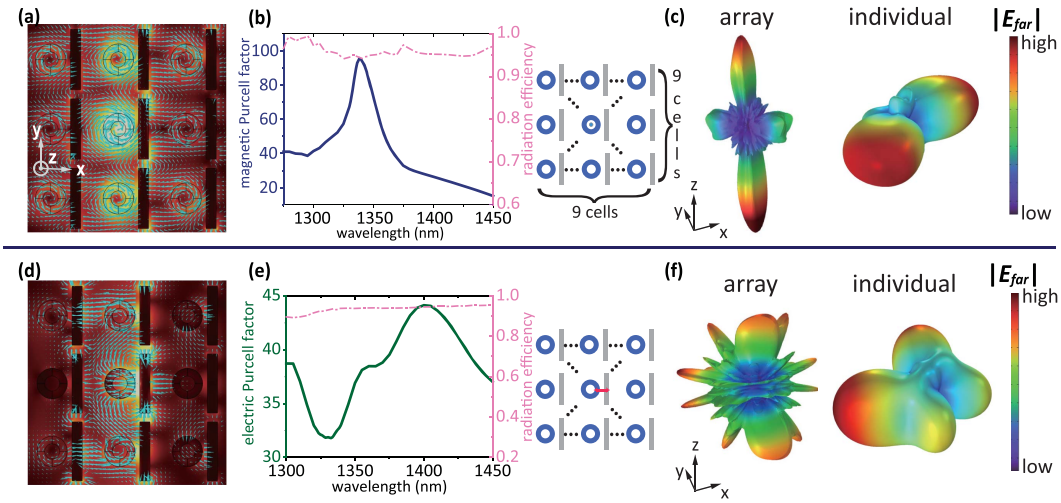

Fig. 4. Purcell enhancement, radiation efficiency, and far-field radiation in a 9 × 9 array of hybrid structures. (a),(d) Field profiles of the array excited by the MQE (or EQE) situated at the central cell. (b),(e) Radiation properties including the magnetic (electric) Purcell factors and the radiation efficiency. The right insets give schematics of the 9 × 9 array excited by the MQE or the EQE. (c),(f) The far-field radiation of the array (or the individual structure) excited by the MQE or the EQE. Compared with the individual structure, the far-field radiation exhibits a more directional pattern.

As shown in the insets of Figs. 4(b) and 4(e), they are located in the central cell. We choose such a size to ensure that the Purcell factor remains at the same level when the array size expands. At the same time, it should not be oversized so that unnecessary calculations can be avoided (see more details in the Supplementary Material).

When the array is excited by the MQE, the advantages manifest in the larger magnetic Purcell enhancement and effective far-field radiation. The maximum Purcell enhancement is close to 100 folds at 1330 nm, higher than that of the individual structure mentioned above. The greater Purcell enhancement can be attributed to the existence of more adjacent structures[54]. For the far-field radiation, the radiation efficiency maintains above 90%. The modulation of the array can be described by an array factor[55], making the far-field radiation exhibit several main lobes and many side lobes. Under the excitation of the MQE, the excitation of each cell is close to the magnetic-like resonance, and the array factor has an approximate form of, $\sin(N\pi d \sin\theta/\lambda)/[N \sin(\pi d \sin\theta/\lambda)]$, where N is the row (or column) count of the array and θ is the radiation direction. The array factor has a strong component in the normal direction. Thus, the radiation [Fig. 4(c)] exhibits a good directional pattern with 70% of the far-field emission radiating into the normal direction.

When the EQE excites the array, the maximum Purcell factor remains at the same level, as compared with an individual structure, and reaches 45 around 1400 nm. In the case of the excitation of EQE, the resonance of each cell is more complicated. In the central cell, the electric-like resonance is excited. In the adjacent and remoter cells, the excitation is relatively weak and more similar with magnetic-like resonance [Fig. 4(d)]. Figure 4(f) depicts the far-field radiation. The enhancement of the array factor is relatively low in the normal direction, making the side lobes obvious[56]. Moreover, the metal absorption is still suppressed. The radiation efficiency also stays above 89%.

5. Conclusion

Here, we propose a hybrid metal-dielectric structure composed of a silicon nanoring and a metal nanorod. The structure supports both large MLDOS and ELDOS, allowing for both a 60-fold magnetic Purcell enhancement and a 45-fold electric Purcell enhancement with a 70-nm gap. Its advantages show in the stronger field confinement and relatively low Ohmic loss when compared to using a single dielectric nanoring or metal nanorod. Moreover, the array that is composed of hybrid structures can modify the emission properties in directional far-field radiation and larger Purcell enhancement.

The structure can be fabricated by current nanofabrication techniques, such as electron beam lithography[22,57]. The emitter can be prepared by doping nanocrystals and then be assembled into the structure using atom force microscopy tips[4]. The hybrid structure also brings conveniences to nanofabrication. The limitation of positioning the emitters can be relaxed because of the high MLDOS and ELDOS in a wide region around the structure. The arrangement is relatively simple and also provides rich parameters to modulate resonances for optical antennas and metasurfaces. The proposed structure provides a wealth of parameters to modulate resonances for optical antennas and light-emitting metasurfaces. By combining the MD and the ED, the EQ resonances in both the dielectric and metal structures, and it can be easily optimized for specifical designs. The magnetic and electric Purcell enhancement also provides a route to selective excitation for photon sources on integrated circuits. Its applications are diverse, from increasing emission rate of

lanthanide ions to enhancing and monitoring photochemical reactions such as photocatalysis.

Acknowledgement

This work was supported by the National Natural Science Foundation of China (Nos. 11974032, 11734001, and 11525414) and the Key R&D Program of Guangdong Province (No. 2018B030329001).

References

1. E. M. Purcell, "Spontaneous emission probabilities at radio frequencies," Phys. Rev. **69**, 37 (1946).
2. P. Albella, M. A. Poyli, M. K. Schmidt, S. A. Maier, F. Moreno, J. J. Sáenz, and J. Aizpurua, "Low-loss electric and magnetic field-enhanced spectroscopy with subwavelength silicon dimers," J. Phys. Chem. C. **117**, 13573 (2013).
3. R. Hussain, S. S. Kruk, C. E. Bonner, M. A. Noginov, I. Staude, Y. S. Kivshar, N. Noginova, and D. N. Neshev, "Enhancing Eu^{3+} magnetic dipole emission by resonant plasmonic nanostructures," Opt. Lett. **40**, 1659 (2015).
4. L. Aigouy, A. Cazé, P. Gredin, M. Mortier, and R. Carminati, "Mapping and quantifying electric and magnetic dipole luminescence at the nanoscale," Phys. Rev. Lett. **113**, 076101 (2014).
5. D. G. Baranov, R. S. Savelev, S. V. Li, A. E. Krasnok, and A. Alù, "Modifying magnetic dipole spontaneous emission with nanophotonic structures," Laser Photon. Rev. **11**, 1600268 (2017).
6. W. T. Carnall, P. R. Fields, and K. Rajnak, "Spectral intensities of the trivalent lanthanides and actinides in solution. II. Pm^{3+}, Sm^{3+}, Eu^{3+}, Gd^{3+}, Tb^{3+}, Dy^{3+}, and Ho^{3+}," J. Chem. Phys. **49**, 4412 (1968).
7. J. R. Zurita-Sánchez and L. Novotny, "Multipolar interband absorption in a semiconductor quantum dot. II. Magnetic dipole enhancement," J. Opt. Soc. Am. B. **19**, 2722 (2002).
8. N. R. Brewer, Z. N. Buckholtz, Z. J. Simmons, E. A. Mueller, and D. D. Yavuz, "Coherent magnetic response at optical frequencies using atomic transitions," Phys. Rev. X. **7**, 011005 (2017).
9. S. M. Hein and H. Giessen, "Tailoring magnetic dipole emission with plasmonic split-ring resonators," Phys. Rev. Lett. **111**, 026803 (2013).
10. X. Fang, M. L. Tseng, D. P. Tsai, and N. I. Zheludev, "Coherent excitation-selective spectroscopy of multipole resonances," Phys. Rev. Appl. **5**, 014010 (2016).
11. H. Sugimoto and M. Fujii, "Magnetic Purcell enhancement by magnetic quadrupole resonance of dielectric nanosphere antenna," ACS Photonics **8**, 1794 (2021).
12. T. Feng, Y. Xu, Z. Liang, and W. Zhang, "All-dielectric hollow nanodisk for tailoring magnetic dipole emission," Opt. Lett. **41**, 5011 (2016).
13. J. Wang, X. Wang, and M. Zeng, "Broadband transverse displacement sensing of silicon hollow nanodisk under focused radial polarization illumination in the near-infrared region," Chin. Opt. Lett. **18**, 063602 (2020).
14. R. M. Bakker, D. Permyakov, Y. F. Yu, D. Markovich, R. Paniagua-Domínguez, L. Gonzaga, A. Samusev, Y. Kivshar, B. Luk'yanchuk, and A. I. Kuznetsov, "Magnetic and electric hotspots with silicon nanodimers," Nano Lett. **15**, 2137 (2015).
15. T. Grosjean, M. Mivelle, F. I. Baida, G. W. Burr, and U. C. Fischer, "Diabolo nanoantenna for enhancing and confining the magnetic optical field," Nano Lett. **11**, 1009 (2011).
16. M. Mivelle, T. Grosjean, G. W. Burr, U. C. Fischer, and M. F. Garcia-Parajo, "Strong modification of magnetic dipole emission through diabolo nanoantennas," ACS Photonics **2**, 1071 (2015).
17. Y. Jia, Y. Ren, X. Zhao, and F. Chen, "Surface lattice resonances in dielectric metasurfaces for enhanced light-matter interaction [Invited]," Chin. Opt. Lett. **19**, 060013 (2021).
18. Y. Sun, V. Yaroshenko, A. Chebykin, E. Ageev, S. Makarov, and D. Zuev, "Metal-dielectric nanoantenna for radiation control of a single-photon emitter," Opt. Mater. Express **10**, 29 (2020).
19. Y. Yang, B. Zhu, and H. Dai, "Strong magnetic field enhancement and magnetic Purcell effect in a dielectric disk-ring composite nanocavity," J. Opt. Soc. Am. B. **37**, 702 (2020).
20. V. F. Gili, L. Ghirardini, D. Rocco, G. Marino, I. Favero, I. Roland, G. Pellegrini, L. Duò, M. Finazzi, L. Carletti, A. Locatelli, A. Lemaître, D. Neshev, C. De Angelis, G. Leo, and M. Celebrano, "Metal–dielectric hybrid nanoantennas for efficient frequency conversion at the anapole mode," Beilstein J. Nanotechnol. **9**, 2306 (2018).
21. S. Sun, M. Li, Q. Du, C. E. Png, and P. Bai, "Metal–dielectric hybrid dimer nanoantenna: coupling between surface plasmons and dielectric resonances for fluorescence enhancement," J. Phys. Chem. C. **121**, 12871 (2017).
22. J. Ho, Y. H. Fu, Z. Dong, R. Paniagua-Dominguez, E. H. H. Koay, Y. F. Yu, V. Valuckas, A. I. Kuznetsov, and J. K. W. Yang, "Highly directive hybrid metal–dielectric Yagi-Uda nanoantennas," ACS Nano. **12**, 8616 (2018).
23. M. A. Schmidt, D. Y. Lei, L. Wondraczek, V. Nazabal, and S. A. Maier, "Hybrid nanoparticle–microcavity-based plasmonic nanosensors with improved detection resolution and extended remote-sensing ability," Nat. Commun. **3**, 1108 (2012).
24. F. Zhang, J. Ren, L. Shan, X. Duan, Y. Li, T. Zhang, Q. Gong, and Y. Gu, "Chiral cavity quantum electrodynamics with coupled nanophotonic structures," Phys. Rev. A. **100**, 053841 (2019).
25. H. M. Doeleman, C. D. Dieleman, C. Mennes, B. Ehrler, and A. F. Koenderink, "Observation of cooperative Purcell enhancements in antenna–cavity hybrids," ACS Nano. **14**, 12027 (2020).
26. L. Shan, J. Ren, Q. Zhang, Q. Liu, Y. Ma, Q. Gong, and Y. Gu, "Generation and modulation of non-classical light in a strongly coupled photon–emitter system," Photonics Res. **10**, 989 (2022).
27. H. Lian, Y. Gu, J. Ren, F. Zhang, L. Wang, and Q. Gong, "Efficient single photon emission and collection based on excitation of gap surface plasmons," Phys. Rev. Lett. **114**, 193002 (2015).
28. L. Shan, F. Zhang, J. Ren, Q. Zhang, Q. Gong, and Y. Gu, "Large Purcell enhancement with nanoscale non-reciprocal photon transmission in chiral gap-plasmon-emitter systems," Opt. Express **28**, 33890 (2020).
29. S. Sarkar, V. Gupta, M. Kumar, J. Schubert, P. T. Probst, J. Joseph, and T. A. F. König, "Hybridized guided-mode resonances via colloidal plasmonic self-assembled grating," ACS Appl. Mater. Interfaces **11**, 13752 (2019).
30. R. F. Oulton, V. J. Sorger, T. Zentgraf, R.-M. Ma, C. Gladden, L. Dai, G. Bartal, and X. Zhang, "Plasmon lasers at deep subwavelength scale," Nature **461**, 629 (2009).
31. H. Li, J.-H. Li, K.-B. Hong, M.-W. Yu, Y.-C. Chung, C.-Y. Hsu, J.-H. Yang, C.-W. Cheng, Z.-T. Huang, K.-P. Chen, T.-R. Lin, S. Gwo, and T.-C. Lu, "Plasmonic nanolasers enhanced by hybrid graphene–insulator–metal structures," Nano Lett. **19**, 5017 (2019).
32. H. Wang, P. Liu, Y. Ke, Y. Su, L. Zhang, N. Xu, S. Deng, and H. Chen, "Janus magneto–electric nanosphere dimers exhibiting unidirectional visible light scattering and strong electromagnetic field enhancement," ACS Nano. **9**, 436 (2015).
33. C. Xu, K. Cheng, Q. Li, X. Shang, C. Wu, Z. Wei, X. Zhang, and H. Li, "The dual-frequency zero-backward scattering realized in a hybrid metallo-dielectric nanoantenna," AIP Adv. **9**, 075121 (2019).
34. T. Shibanuma, G. Grinblat, P. Albella, and S. A. Maier, "Efficient third harmonic generation from metal–dielectric hybrid nanoantennas," Nano Lett. **17**, 2647 (2017).
35. J. Shi, Y. Li, M. Kang, X. He, N. J. Halas, P. Nordlander, S. Zhang, and H. Xu, "Efficient second harmonic generation in a hybrid plasmonic waveguide by mode interactions," Nano Lett. **19**, 3838 (2019).
36. D. Ray, T. V. Raziman, C. Santschi, D. Etezadi, H. Altug, and O. J. F. Martin, "Hybrid metal-dielectric metasurfaces for refractive index sensing," Nano Lett. **20**, 8752 (2020).
37. Z. Qian, L. Shan, X. Zhang, Q. Liu, Y. Ma, Q. Gong, and Y. Gu, "Spontaneous emission in micro- or nanophotonic structures," PhotoniX **2**, 21 (2021).
38. Q. Li, D. Pan, H. Wei, and H. Xu, "Plasmon-assisted selective and super-resolving excitation of individual quantum emitters on a metal nanowire," Nano Lett. **18**, 2009 (2018).
39. A. Manjavacas, R. Fenollosa, I. Rodriguez, M. C. Jiménez, M. A. Miranda, and F. Meseguer, "Magnetic light and forbidden photochemistry: the case of singlet oxygen," J. Mater. Chem. C. **5**, 11824 (2017).
40. H. Sugimoto, H. Hasebe, T. Furuyama, and M. Fujii, "Direct excitation of triplet state of molecule by enhanced magnetic field of dielectric metasurfaces," Small **17**, 2104458 (2021).

41. A. G. Curto, G. Volpe, T. H. Taminiau, M. P. Kreuzer, R. Quidant, and N. F. Van Hulst, "Unidirectional emission of a quantum dot coupled to a nanoantenna," Science **329**, 930 (2010).
42. P. B. Johnson and R. W. Christy, "Optical constants of the noble metals," Phys. Rev. B. **6**, 4370 (1972).
43. J.-H. Yang and K.-P. Chen, "Hybridization of plasmonic and dielectric metasurfaces with asymmetric absorption enhancement," J. Appl. Phys. **128**, 133101 (2020).
44. S. Sun, T. Zhang, Q. Liu, L. Ma, Q. Du, and H. Duan, "Enhanced directional fluorescence emission of randomly oriented emitters via a metal–dielectric hybrid nanoantenna," J. Phys. Chem. C. **123**, 21150 (2019).
45. L. Cui, M.-Y. Huang, Y.-M. You, G.-M. Li, Y.-J. Zhang, C.-K. Liu, and S.-L. Liu, "Enhancement of magnetic dipole emission at yellow light with polarization-independent hexagonally arrayed nanorods optical metamaterials," Opt. Mater. Express **6**, 1151 (2016).
46. J. T. Hugall, A. Singh, and N. F. Van Hulst, "Plasmonic cavity coupling," ACS Photonics **5**, 43 (2018).
47. J. J. Baumberg, J. Aizpurua, M. H. Mikkelsen, and D. R. Smith, "Extreme nanophotonics from ultrathin metallic gaps," Nat. Mater. **18**, 668 (2019).
48. J. van de Groep and A. Polman, "Designing dielectric resonators on substrates: combining magnetic and electric resonances," Opt. Express **21**, 26285 (2013).
49. P. Spinelli, C. van Lare, E. Verhagen, and A. Polman, "Controlling Fano lineshapes in plasmon-mediated light coupling into a substrate," Opt. Express **19**, A303 (2011).
50. H.-W. Wu, Y. Li, H.-J. Chen, Z.-Q. Sheng, H. Jing, R.-H. Fan, and R.-W. Peng, "Strong Purcell effect for terahertz magnetic dipole emission with spoof plasmonic structure," ACS Appl. Nano Mater. **2**, 1045 (2019).
51. W. Hu, N. Yi, S. Sun, L. Cui, Q. Song, and S. Xiao, "Enhancement of magnetic dipole emission at yellow light in optical metamaterials," Opt. Commun. **350**, 202 (2015).
52. K. J. Savage, M. M. Hawkeye, R. Esteban, A. G. Borisov, J. Aizpurua, and J. J. Baumberg, "Revealing the quantum regime in tunnelling plasmonics," Nature **491**, 574 (2012).
53. T. Takeuchi, M. Noda, and K. Yabana, "Operation of quantum plasmonic metasurfaces using electron transport through subnanometer gaps," ACS Photonics **6**, 2517 (2019).
54. K. Du, P. Li, H. Wang, K. Gao, R. B. Liu, F. Lu, W. Zhang, and T. Mei, "Optical chirality enhancement in hollow silicon disk by dipolar interference," Adv. Opt. Mater. **9**, 2001771 (2021).
55. C. A. Balanis, *Antenna Theory: Analysis and Design*, 4th ed. (Wiley, 2005).
56. A. Vaskin, R. Kolkowski, A. F. Koenderink, and I. Staude, "Light-emitting metasurfaces," Nanophotonics **8**, 1151 (2019).
57. Y. Yang, I. I. Kravchenko, D. P. Briggs, and J. Valentine, "All-dielectric metasurface analogue of electromagnetically induced transparency," Nat. Commun. **5**, 5753 (2014).